



Original Article



Natural convection of rectangular cavity enhanced by obstacle and fin to simulate phase change material melting process using Lattice Boltzmann method

Gongxing Yan^{a,b}, As'ad Alizadeh^{c,*}, Amin Rahmani^d, Majid Zarringhalam^e, Mahmoud Shamsborhan^f, Navid Nasajpour-Esfahani^g, Mohammad Akrami^d

^a School of Intelligent Construction, Luzhou Vocational and Technical College, Luzhou 646000, Sichuan, China

^b Luzhou Key Laboratory of Intelligent Construction and Low-carbon Technology, Luzhou 646000, Sichuan, China

^c Department of Civil Engineering, College of Engineering, Cihan University-Erbil, Erbil, Iraq

^d Department of Engineering, University of Exeter, Exeter EX4 4QF, UK

^e Young Researchers and Elite Club, South Tehran Branch, Islamic Azad University, Tehran, Iran

^f Department of Mechanical Engineering, College of Engineering, University of Zakho, Zakho, Iraq

^g Department of Material Science and Engineering, Georgia Institute of Technology, Atlanta 30332, USA

ARTICLE INFO

Keywords:

Lattice Boltzmann Method
Phase change material
Adiabatic fin
Adiabatic obstacle
Fluid fraction diagram

ABSTRACT

In recent years, the lattice Boltzmann method has become a powerful method for computational modeling of various complex fluid flow concerns, including the simulation of the melting process in phase change materials. In the present paper, the natural convection of phase change materials in a cavity is simulated, and the effect of adiabatic obstacle and fin is investigated by the lattice Boltzmann method. The obtained results are presented in different Rayleigh numbers ($Ra = 10^3$ - 10^5), and cavity angles ($\theta = -90$ to 90) in three scenarios (without adiabatic fin and obstacle, with an adiabatic obstacle, and with adiabatic fin). The investigation across various cavity angles, with adiabatic obstacles and fins, demonstrates a consistent trend of effective melting process delay by up to 50%, underscoring the significant impact of these adiabatic features on PCM behavior. Adiabatic obstacles induce localized melting delays due to unmelted zones around them. Streamlines highlight vortices formed by obstacles, and elevated Nusselt numbers correlate with accelerated melting facilitated by adiabatic fins. Modifying the adiabatic fin height from $Y_f = 0.1$ to $Y_f = 0.7$ leads to a doubling of melting time at around 80% PCM melting. Conversely, decreasing fin height from 0.5 to 0.7 extends the complete melting time by approximately 10%, showcasing the influential role of fin height in shaping PCM melting behaviour.

1. Introduction

Enhancing the heat transfer of fluids is a topic of great interest for various industrial and engineering problems [1]. Due to their ability to store and release thermal energy during phase transitions, the use of Phase Change Materials (PCMs) has attracted considerable interest in recent years for various engineering applications [2]. The melting process, which has applications varying from renewable energy storage systems to electronic cooling, is a crucial procedure in which PCMs play a crucial role [3,4]. A prospective method for enhancing the PCM melting process is to incorporate an obstacle and a fin to enhance the natural convection within a rectangular cavity. Computational methods, such as the Lattice Boltzmann Method (LBM), have emerged as effective

instruments for analyzing complex fluid flow and heat transfer phenomena [5–9].

Researchers have explored various aspects of phase change and heat transfer using the Lattice Boltzmann Method (LBM) in different configurations [10,11]. Shojaeefard et al. [12] investigated thermal storage efficiency using LBM, incorporating hybrid nanofluids to enhance melting in a rectangular system cooled by an intruded T-shaped cavity, finding silica-MWCNT NPs/water composite with a volume fraction of 0.01 most effective. Farhadi et al. [8] explored heat transfer enhancement by a porous medium in a ventilated cavity using LBM, demonstrating improved heat transfer with decreased porosity and higher Reynolds and Prandtl numbers. Another study by Shojaeefard et al. [13] examined ice melting in a square cavity with partially active walls,

* Corresponding author.

E-mail addresses: yaangx@126.com (G. Yan), asad.alizadeh2010@gmail.com (A. Alizadeh).

<https://doi.org/10.1016/j.aej.2023.09.035>

Received 20 March 2023; Received in revised form 10 August 2023; Accepted 9 September 2023

Available online 18 September 2023

1110-0168/© 2023 THE AUTHORS. Published by Elsevier BV on behalf of Faculty of Engineering, Alexandria University. This is an open access article under the CC BY-NC-ND license (<http://creativecommons.org/licenses/by-nc-nd/4.0/>).

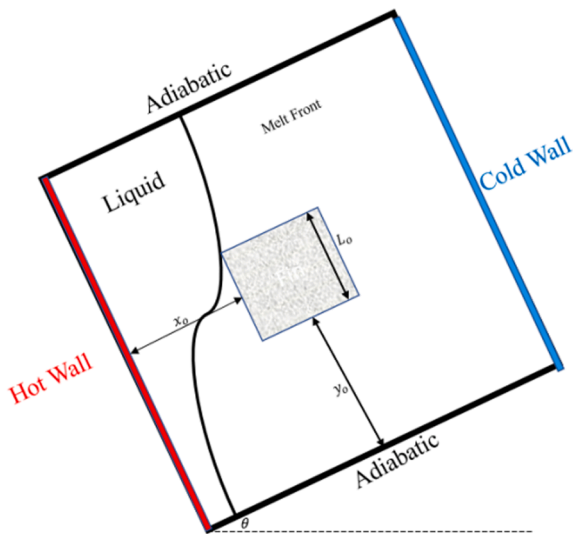


Fig. 1. Schematic geometry of this study (Obstacle).

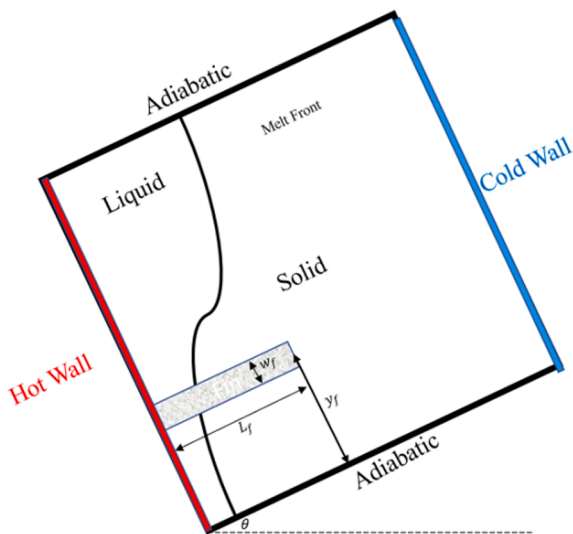


Fig. 2. Schematic geometry of this study (Fin).

Table 1
Thermophysical properties of Paraffin-Wax (PCM) [28].

Properties	Paraffin-Wax
c_p (J/kg.K)	1868
ρ (kg/m ³)	950
k (W/mK)	0.2
T_m (K)	350.15
Latent heat of Fusion (KJ/Kg)	176

proposing hybrid nanoparticles for thermal energy storage enhancement, highlighting the influence of nanoparticle type, proportions, and active part positions on efficiency.

In their work, Liu et al. [14] introduced an enthalpy-based immersed boundary-lattice Boltzmann model to study solid–liquid phase change in porous media under the Local Thermal Non-Equilibrium (LTNE) condition. The proposed model addressed numerical diffusion across the phase interface using an enthalpy-based TRT-LB model for solid–liquid phase change under LTNE. Additionally, the non-slip boundary condition on the phase interface was handled using the partially saturated method. These features were implemented to enhance the accuracy and

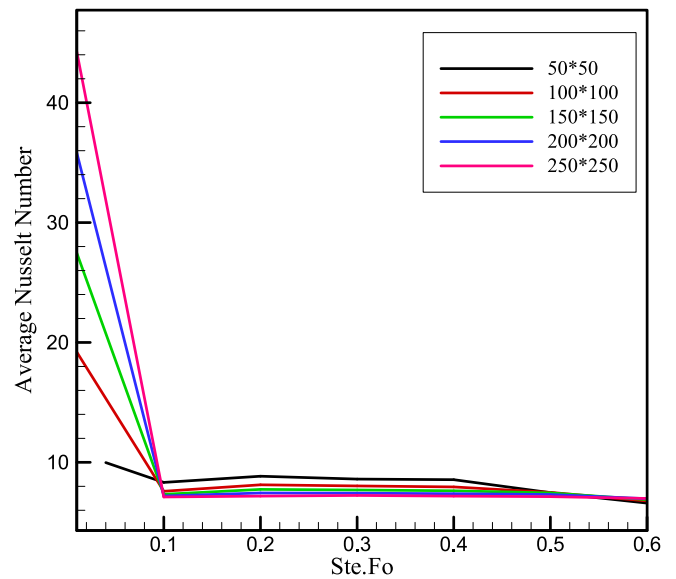


Fig. 3. Grid study on 100 × 100, 120 × 120, 200 × 200, and 250 × 250 lattices.

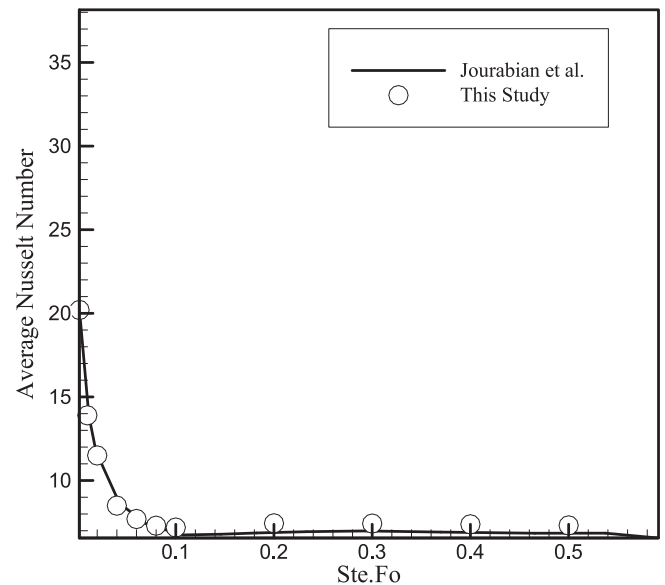


Fig. 4. Comparison of the average Nusselt number at $Ra = 1.7 \times 10^5$ between this study and results of Jourabian et al. [31].

reliability of simulations in the context of solid–liquid phase change in porous media.

Laouer get al. [15] investigated the effects of nanoparticle loading, fin utilization, and the combined use of nanoparticles and fins on the heat transfer and melting of PCM. Their findings revealed that a nanoparticle concentration of 6% significantly decreased the total melting time of HPCM by 12.8%. Moreover, attaching a single fin within the cavity resulted in a notable 15.3% increase in liquid fraction, whereas increasing the fin length ratio accelerated the melting time by a remarkable 64.0%. This study intends to contribute to developing effective cold energy storage systems by extending their research on heat transfer enhancement techniques.

Souayfane et al. [16] presented a simplified model for investigating PCM melting via natural convection and radiation. The model demonstrates high precision and computational efficiency using a modified enthalpy method, an improved thermal conductivity approach, and a

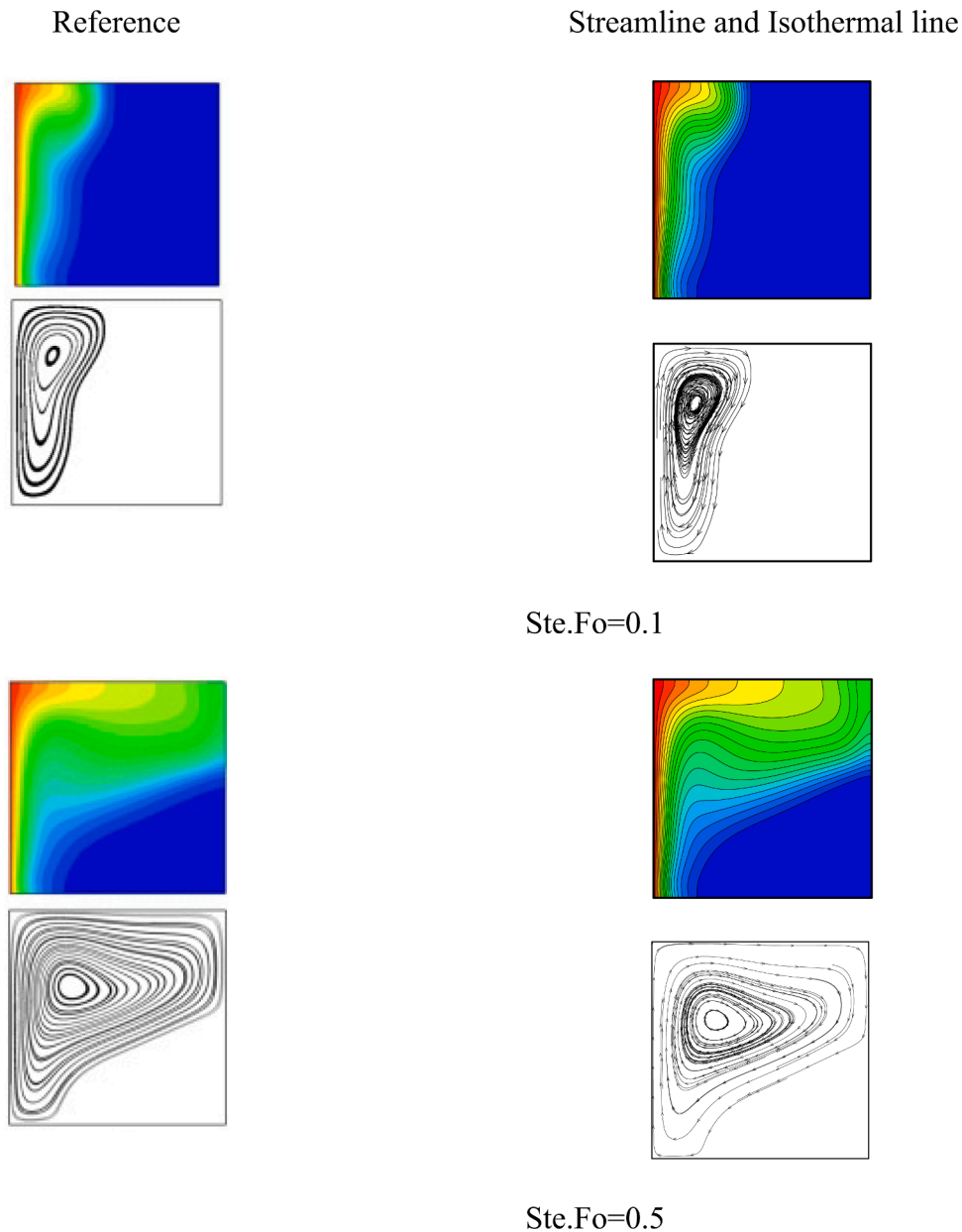


Fig. 5. Comparison of the isothermal lines and streamlines obtained in this research and the results of Jourabian et al. [31].

simplified solution algorithm for absorbed shortwave radiation. The study provides vital insights for optimizing PCM utilization in various thermal applications. Many other research field can be found in the literature [17,18,19,20].

Building upon these investigations, the effect of obstacles on PCM melting processes has been a focus of exploration. The findings from studies on obstacle-enhanced melting dynamics and the insights gained from Lattice Boltzmann Method simulations contribute to a comprehensive understanding of how geometrical features impact phase change behaviors and heat transfer rates within PCM systems [20,21].

Zhao et al. [22] investigated the effect of a hot obstacle on the melting of PCM using LBM. They reported the size of a hot obstacle as an important parameter of melting rate. They also reported that moving down the position of a hot obstacle can change the heat transfer regime from conduction to convection. Furthermore, the utilization of the Lattice Boltzmann Method (LBM) for investigating the impact of obstacles on the melting process of Phase Change Materials (PCMs) has been explored by other researchers as well [23,24].

Adding components such as fins can enhance heat transfer and influence the phase change of PCMs, leading to accelerated melting processes. Applying the Lattice Boltzmann Method (LBM) has proven effective in studying these systems, offering significant performance benefits. For example, Ren and Chan [25] utilized LBM to simulate PCM melting in an enclosure with internal fins. They observed that increasing the length of the fins could modify the melting rate, but there was a limit to the acceleration achieved by lengthening the fins. Moreover, using longer fins resulted in a decrease in the total final liquid value. The study also explored the influence of the number of fins on the melting process.

Talati and Taghilo [26] conducted a numerical simulation of the solidification process within a rectangular fined container using the implicit lattice Boltzmann method. They studied two problems, the first being the solidification of the phase change material (PCM) within the container with constant temperature on the walls. By implementing the LBM, they provided a method to assess the accuracy of the approximate analytical solution for the solidification problem.

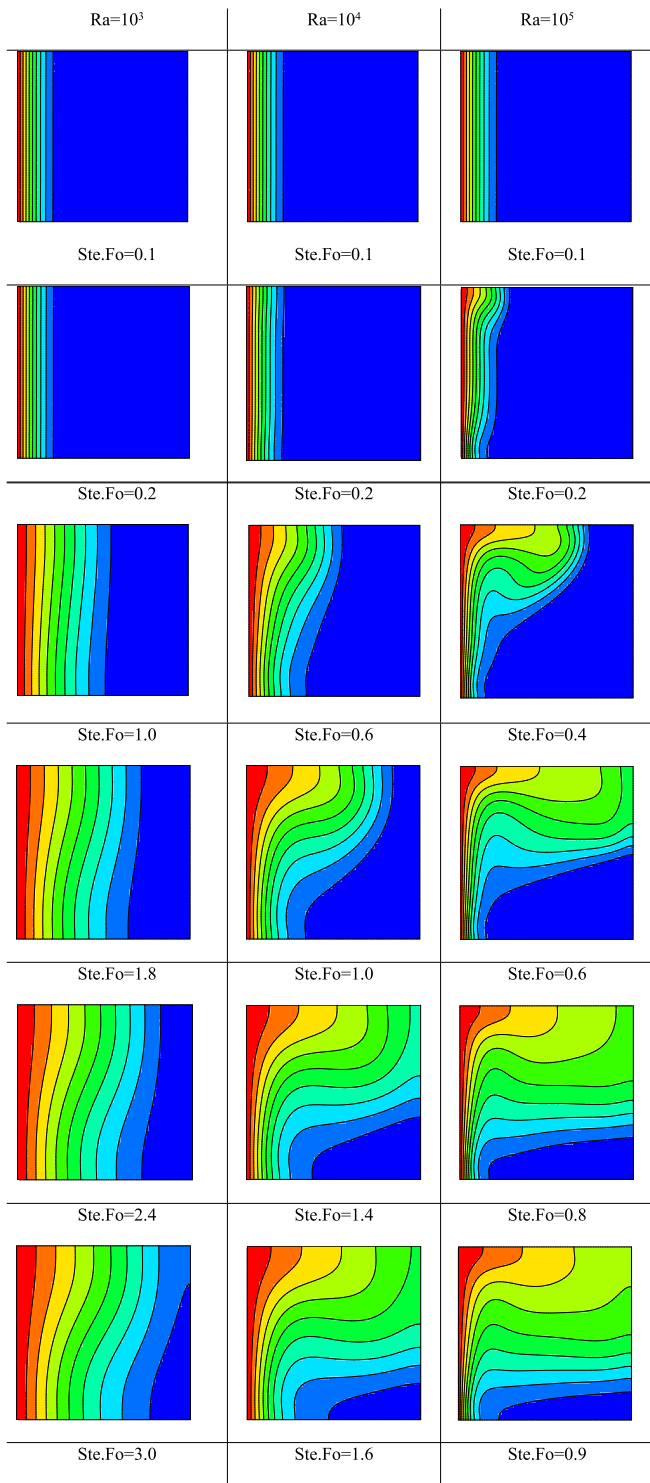


Fig. 6. Isotherms in $Ra = 10^3$ to $Ra = 10^5$ and the cavity angle is zero without the presence of fin and adiabatic obstacle.

Rui et al. [27] utilized the Lattice Boltzmann Method to investigate the effectiveness of the phase change pin fin heat sink for thermal management in electronic equipment and batteries. They evaluated various factors influencing passive heat dissipation performance, such as fin geometry, fin number, fin arrangement, and different phase change materials. They employed a neural network coupled genetic algorithm to optimize the heat sink's structure.

Utilizing the Lattice Boltzmann Method, we delve into the natural convection process within a rectangular cavity containing a phase

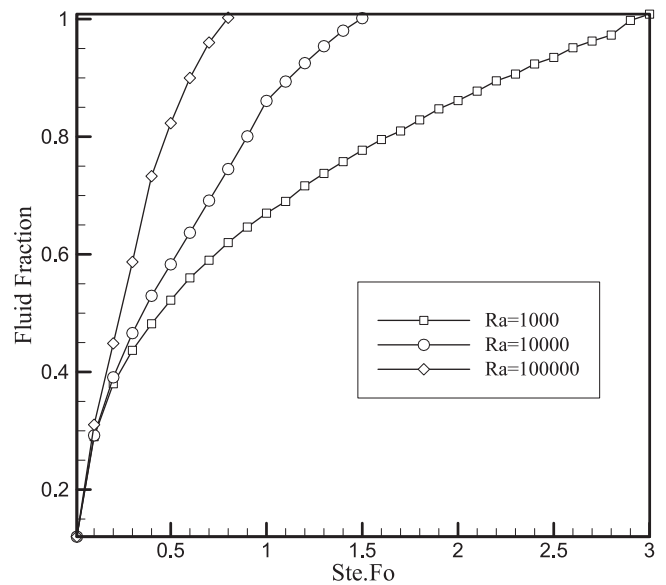


Fig. 7. Melting rate diagram according to $Ste.Fo$ number in $Ra = 10^3$ to $Ra = 10^5$ and the cavity in line with the horizon without the presence of fin and obstacle.

change material (PCM) in this study. Our investigation centres on unravelling the influence of obstacles and fins on the PCM melting process. Notably, our study uniquely addresses the effect of adiabatic fins, filling a gap in the existing literature where previous works mainly focused on hot and thermal fins and obstacles. This numerical exploration yields insightful implications for refining and optimizing thermal management systems and energy storage applications employing PCMs. These outcomes serve to advance the efficiency, effectiveness, and reliability of such systems, thereby fostering sustainable and enhanced thermal energy storage solutions across diverse industries and applications.

2. Problem statement

2.1. Geometry

The natural convection of a cavity containing PCMs was examined as the key challenge tackled in this thesis. This cavity contains two fixed adiabatic walls at the top and bottom and a hot and cold wall on the left and right sides. PCM is affected by the left side wall and starts to melt from the left. The slope of the chamber is θ relative to the horizon, and the position of the adiabatic obstacle is represented by the parameters x_o and y_o , with L_o introducing the length of the cavity. The parameters Y_f and L_f also show the position and size of the adiabatic fin. Figs. 1 and 2 depict the geometry utilized in the issues tackled in this thesis.

In this article, paraffin-wax is used as PCM. Table 1 lists the thermo-physical characteristics of the PCM.

2.2. Governing equations

The governing equations, including continuity, momentum, and energy, are described below [20].

$$\nabla \cdot \vec{u} = 0 \tag{1}$$

$$\frac{\partial \vec{u}}{\partial t} + \vec{u} \cdot (\nabla \cdot \vec{u}) = -\nabla p + \nu \nabla^2 \vec{u} - \vec{g} \beta (T - T_0) \tag{2}$$

$$\frac{\partial T}{\partial t} + \vec{u} \cdot (\nabla T) = \alpha \nabla^2 T - \frac{L_f}{\rho c_p} \frac{\partial F_i}{\partial t} \tag{3}$$

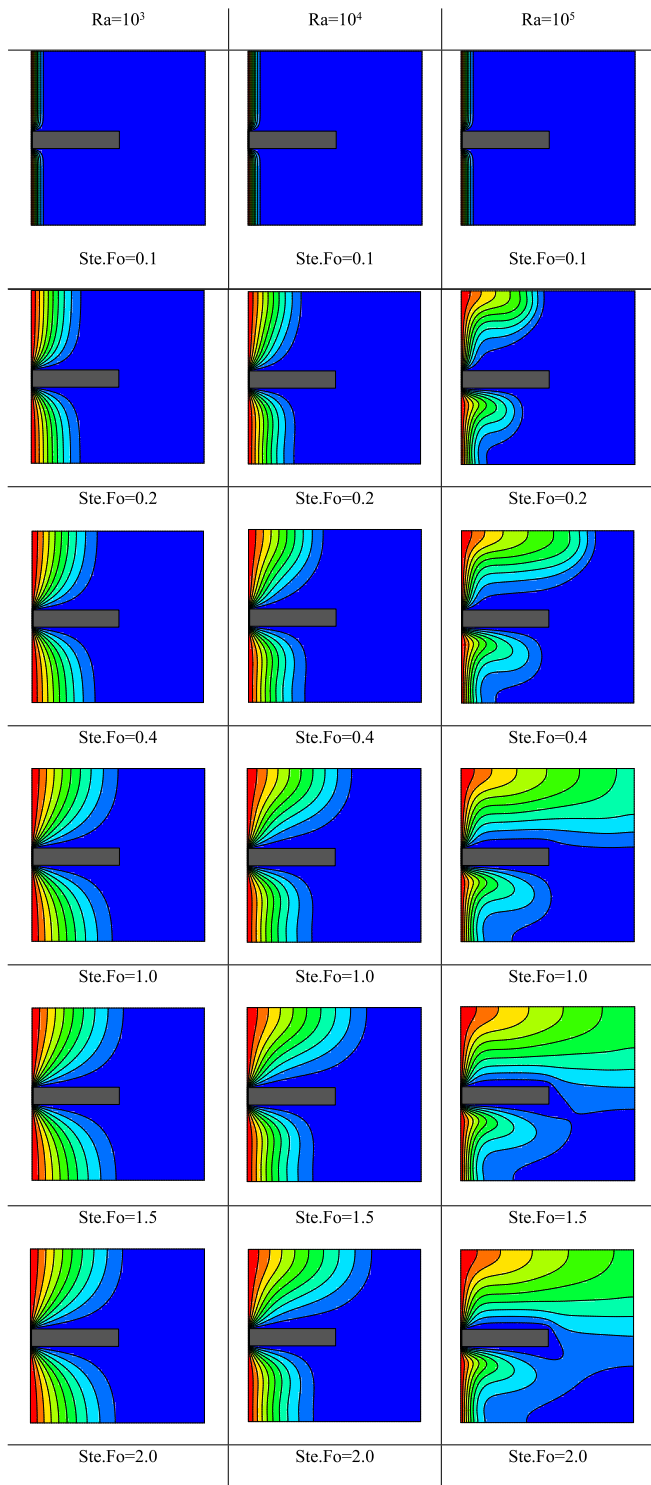


Fig. 8. Isotherms in $Ra = 10^3$ to $Ra = 10^5$ and the cavity angle is zero in the presence of the adiabatic fin.

P stands for pressure, and c_p represents the heat capacity at constant pressure. To resolve the problem under usual circumstances, it is crucial to create a set of dimensionless numbers and variables described below.

$$T^* = \frac{T - T_0}{T_h - T_c} \quad (4)$$

$$Fo = \frac{t\alpha}{H^2} \quad (5)$$

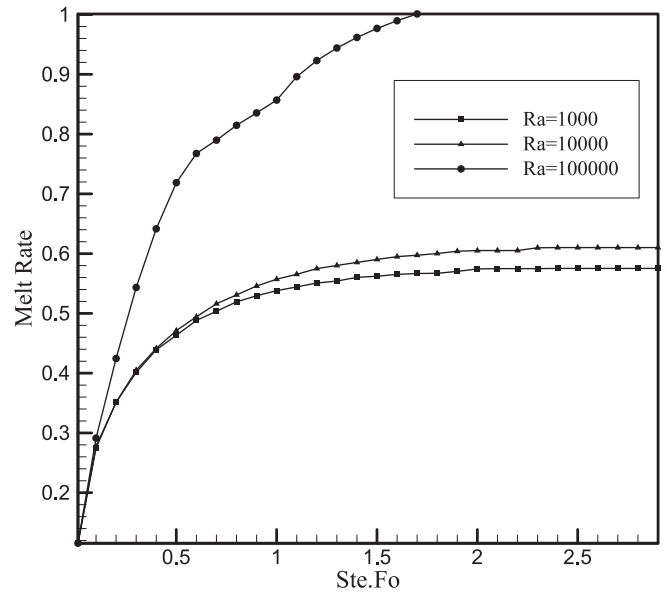


Fig. 9. Melting rate diagram according to $Ste.Fo$ number in $Ra = 10^3$ to $Ra = 10^5$ and the cavity in line with the horizon in presence of fin.

$$x^* = \frac{x}{L} \quad (6)$$

$$y^* = \frac{y}{H} \quad (7)$$

$$Ste = \frac{c_p(T_h - T_c)}{L_f} \quad (8)$$

$$Ra = \frac{\vec{g}\beta(T_h - T_c)H^3}{\alpha\nu} \quad (9)$$

$$\vec{u}^* = \frac{\vec{u}L}{\alpha} \quad (10)$$

$$\vec{v}^* = \frac{\vec{v}H}{\alpha} \quad (11)$$

Using the definitions and justifications provided, the governing equations are recast as follows.

$$\nabla \cdot \vec{u}^* = 0 \quad (12)$$

$$\frac{\partial \vec{u}^*}{\partial t^*} + \vec{u}^* \cdot (\nabla \cdot \vec{u}^*) = -\nabla p^* + Pr \nabla^2 \vec{u}^* - Pr Ra \beta T^* \quad (13)$$

$$\frac{\partial T^*}{\partial t^*} + \vec{u}^* \cdot (\nabla T^*) = \alpha \nabla^2 T^* - \frac{1}{Ste} \frac{\partial F_i}{\partial t^*} \quad (14)$$

2.2.1 Initial conditions

To initialize parameters before starting the simulations, T^* as the dimensionless temperature is set to zero in all the domains except hot wall in Fig. 2 which is $T^* = 1$. Also u^* is set to 0 throughout the domain.

The Boussinesq approximation is utilized to account for density variations in the fluid due to temperature changes. In this study, the only external force applied to the geometry is gravity, and the Boussinesq approximation is considered to accurately model the thermal buoyancy effects caused by temperature gradients.

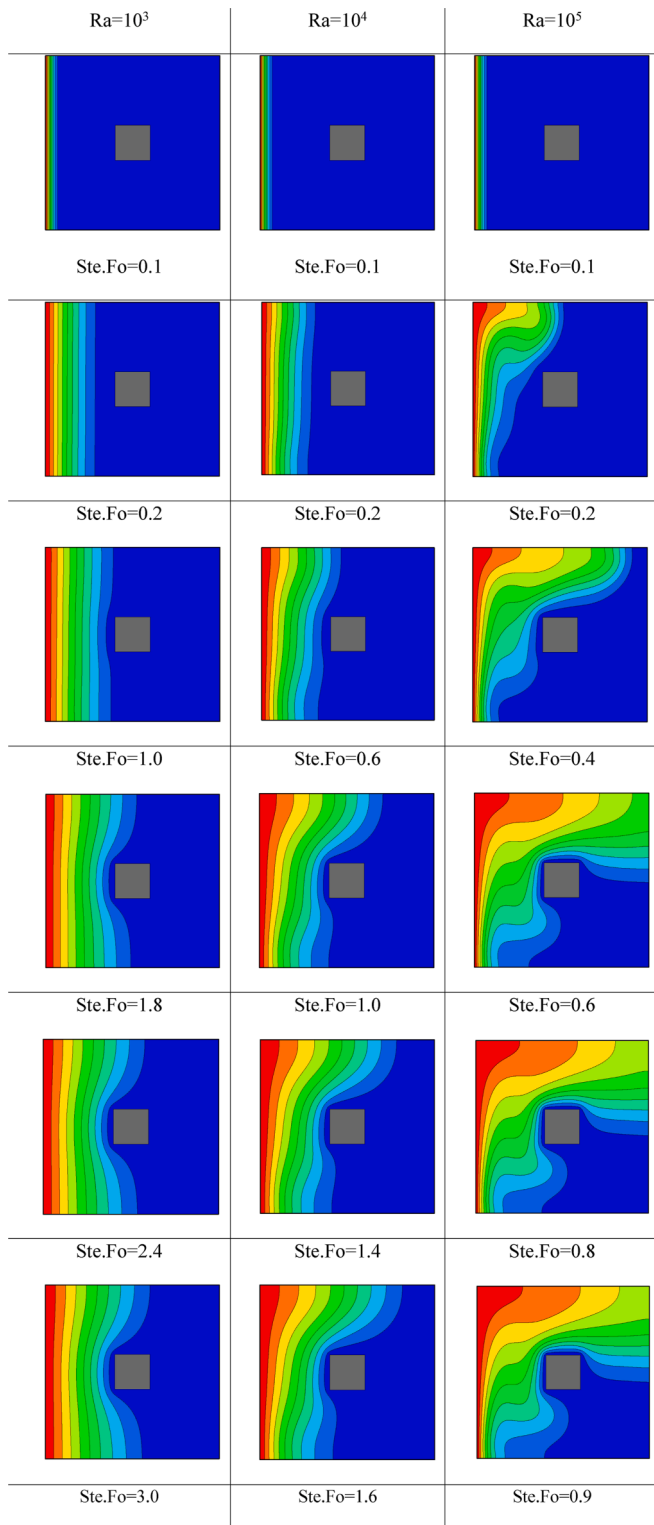


Fig. 10. Isotherms at Ra = 10³ to Ra = 10⁵ and the cavity angle is zero in the presence of the adiabatic obstacle.

2.3. Lattice Boltzmann method

The LBM requires two distribution functions (f and g) for the momentum and energy equations to recover equations (12)–(14). In this section, the LBM equations for the flow and temperature fields are given, and it is shown how LBM can calculate the density, velocity, and temperature as macroscopic quantities [29].

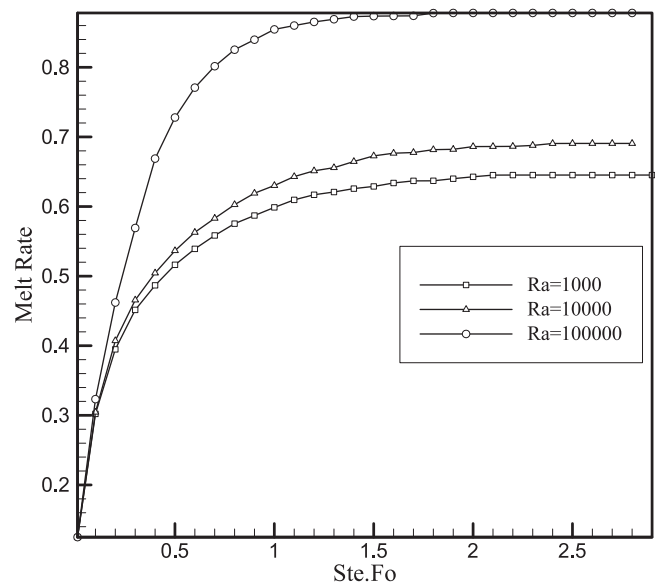


Fig. 11. Melting rate diagram according to Ste.Fo number in Ra = 10³ to Ra = 10⁵ and the cavity in line with the horizon in presence of the obstacle.

$$f_i(\vec{x} + c_i \Delta t, t + \Delta t) = f_i(\vec{x}, t) + \frac{\Delta t}{\tau_v} [f_i^{eq}(\vec{x}, t) - f_i(\vec{x}, t)] + \Delta t c_i F_i \quad (15)$$

$$g_i(\vec{x} + c_i \Delta t, t + \Delta t) = g_i(\vec{x}, t) + \frac{\Delta t}{\tau_D} [g_i^{eq}(\vec{x}, t) - g_i(\vec{x}, t)] - w_i \frac{1}{Ste} (f_i^{n,k} - f_i^{n-1}) \quad (16)$$

For the momentum and energy equations, respectively, τ_v and τ_D are relaxation times that are related to viscosity and heat diffusivity and are specified as [29]:

$$\tau_v = 3\nu + 1/2 \quad (17)$$

$$\tau_D = 3\alpha_{nf} + 0.5 \quad (18)$$

f_i^{eq} and g_i^{eq} are equilibrium distribution functions in direction of i and are defined as [29]:

$$f_i^{eq} = w_i \rho_{nf} \left[1 + \frac{\vec{c}_i \cdot \vec{u}}{c_s^2} + \frac{1}{2} \frac{(\vec{c}_i \cdot \vec{u})^2}{c_s^4} - \frac{1}{2} \frac{u^2}{c_s^2} \right] \quad (19)$$

$$g_i^{eq} = w_i T \left[1 + \frac{\vec{c}_i \cdot \vec{u}}{c_s^2} \right] \quad (20)$$

For the momentum equation a D₂Q₉ and for energy equation a D₂Q₅ lattice structure is used.

w_i is a weighting factor, ρ_{nf} is the density of nanofluid, u is macroscopic velocity, T is temperature and c_i is the microscopic velocity in i direction. w_i and c_i for D₂Q₉ lattice structure is defined as [29]:

$$c_i = \begin{bmatrix} 0 & 1 & 0 & -1 & 0 & 1 & -1 & -1 & 1 \\ 0 & 0 & 1 & 0 & -1 & 1 & 1 & -1 & -1 \end{bmatrix} \quad (21)$$

$$w_i = \begin{bmatrix} 4 & 1 & 1 & 1 & 1 & 4 & 4 & 4 & 4 \\ 9 & 9 & 9 & 9 & 9 & 9 & 9 & 9 & 9 \end{bmatrix} \quad (22)$$

And for D₂Q₅ [29]:

$$c_i = \begin{bmatrix} 0 & 1 & 0 & -1 & 0 \\ 0 & 0 & 1 & 0 & -1 \end{bmatrix} \quad (23)$$

$$w_i = \begin{bmatrix} 4 & 1 & 1 & 1 & 1 \\ 6 & 12 & 12 & 12 & 12 \end{bmatrix} \quad (24)$$

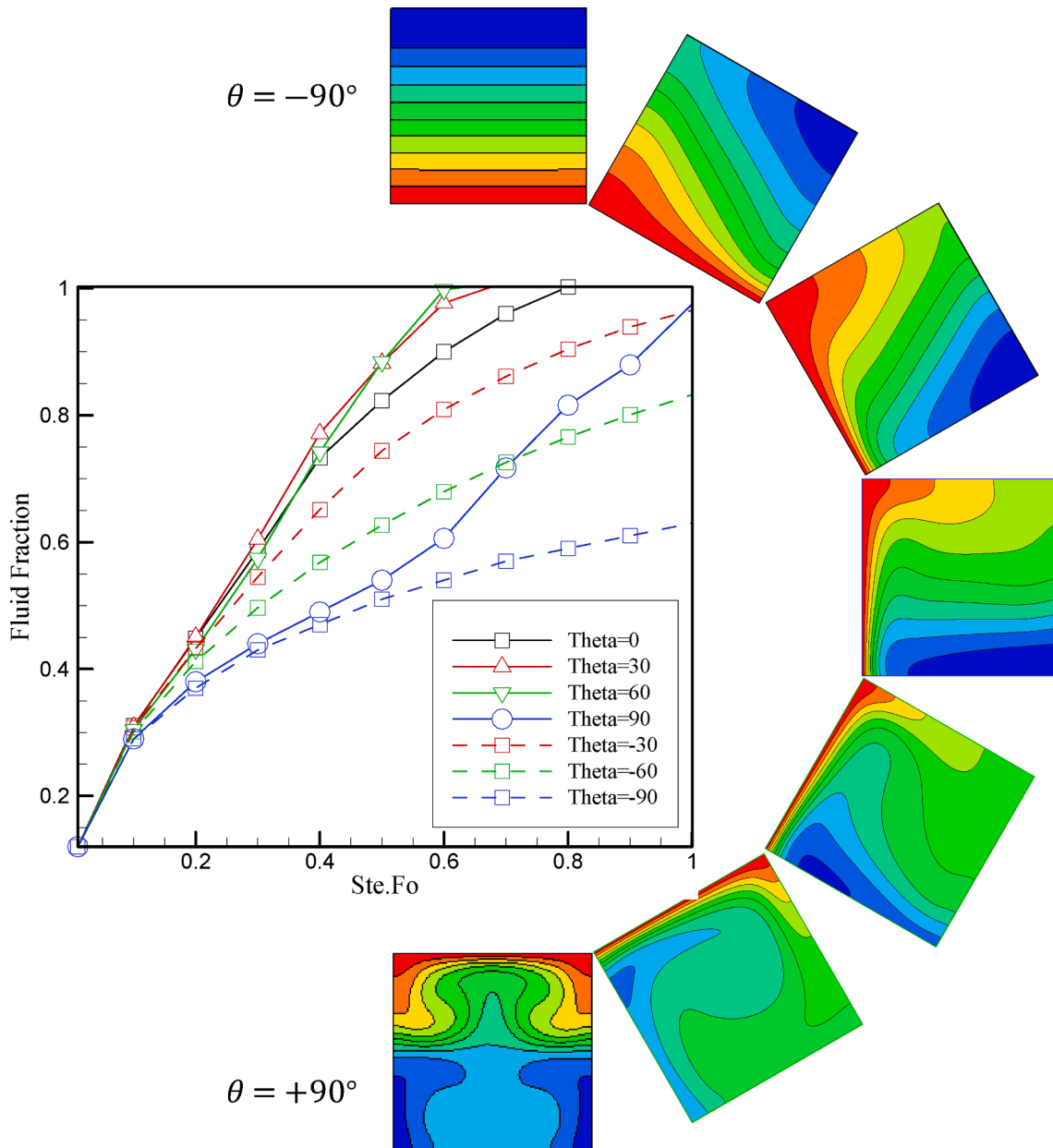


Fig. 12. Isotherms at $Ra = 10^5$ at different angles $\theta = -90^\circ$ to 90° in an adiabatic cavity without fin and obstacle.

A significantly modified version of Jiaung et al. [30]’s melting method was used to tackle the phase change problem. Both the temperature and the liquid fraction were calculated using the enthalpy method. The phase change front is not specifically pursued while using the enthalpy approach. As an alternative, each cell is given a size called the liquid fraction, which represents the percentage of the cell’s volume that is in liquid form. Based on the enthalpy value, the liquid fraction is determined after each repetition. The phase change front’s prerequisites are therefore automatically met. Additionally, a soft zone is produced where the liquid percentage ranges from 0 to 1. Some discontinuities that might cause numerical instability are avoided in this zone. The iteration k is assessed as follows:

$$E^{n,k} = c_p T^{n,k} + L_f f_i^{n,k-1} \tag{25}$$

The liquid fractions are then updated for the current iteration level [31]:

$$f_i^{n,k} = \left\{ \begin{array}{lll} 0 & E_n^{n,k} < E_{n_s} = c_p T_m & \text{solid zone} \\ \frac{E_n^{n,k} - E_{n_s}}{E_{n_l} - E_{n_s}} & E_{n_s} \leq E_n^{n,k} \leq E_{n_s} + L_f & \text{mushy zone} \\ 1 & E_n^{n,k} > E_{n_s} + L_f & \text{liquid zone} \end{array} \right\} \tag{26}$$

where T_m is the melting temperature. Afterward, the temperature distribution functions are acquired by Eq. (16). f and g values may be derived at every point and direction of the fluid domain by solving Eqs. (15) and (16) in collision and streaming stages. These equations may thus be used to compute velocity, density, and temperature [29].

$$\rho_{nf} = \sum_i f_i \tag{27}$$

$$\rho_{nf} \vec{u} = \sum_i \vec{c}_i f_i \tag{28}$$

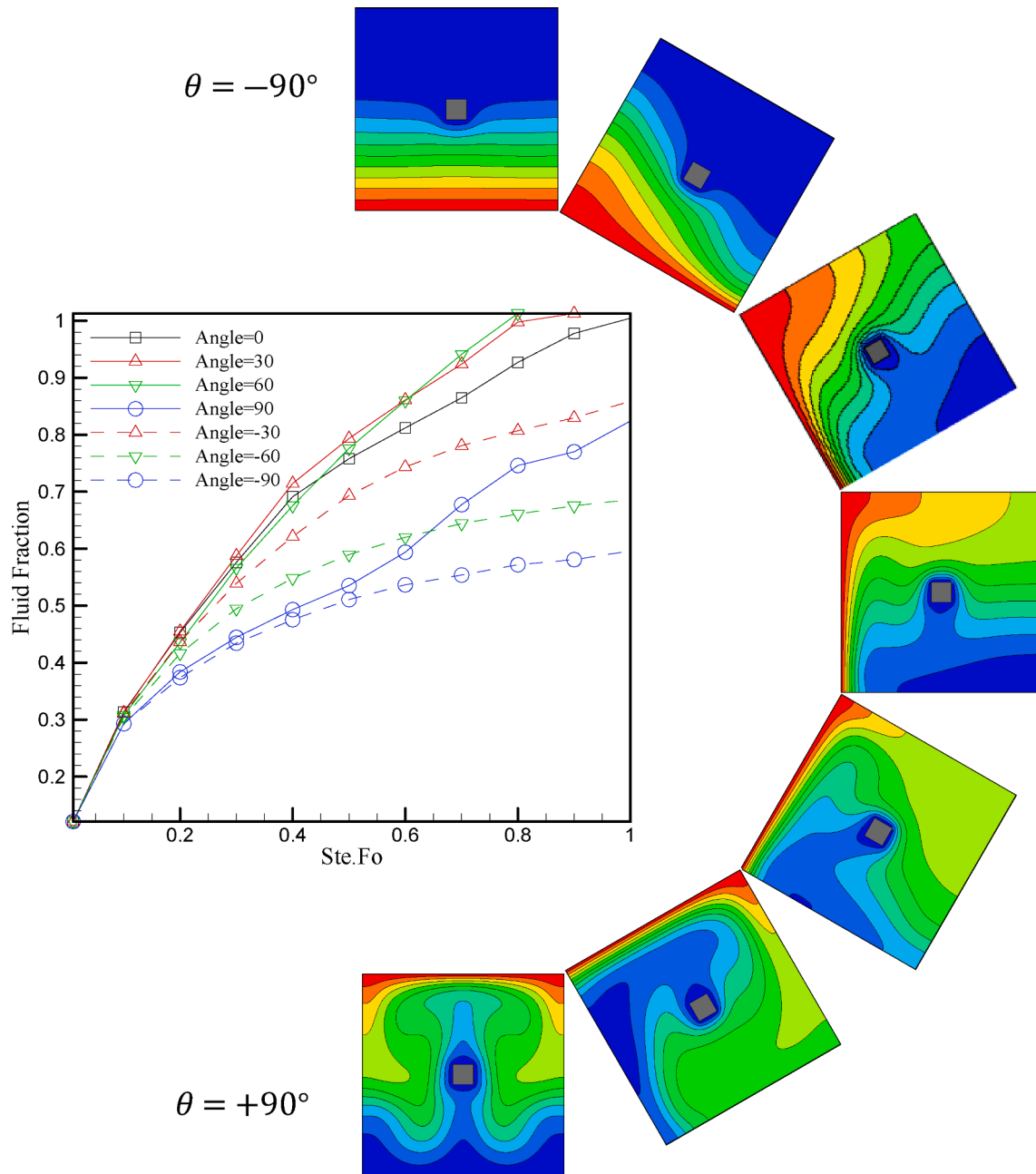


Fig. 13. Isotherms at $Ra = 10^5$ at different angles $\theta = -90^\circ$ to 90° in an adiabatic cavity with an obstacle in the middle.

$$T = \sum_i g_i \tag{29}$$

2.4. Boundary conditions

Many boundary conditions are employed in this technique to mimic the LBM PCM melting issue. Here are the utilized boundary conditions are provided.

1- Flow:

All walls in this simulation are considered to be stationary. To simulate these walls a bounce back boundary condition is employed which is formulized like this:

$$f_i(\vec{x}, t) = f_{\tilde{i}}(\vec{x}, t) \tag{30}$$

Which \tilde{i} is the opposite direction of i .

2- Temperature:

The walls in this simulation are considered to be in a constant temperature or to be adiabatic. To simulate the constant temperature walls:

$$g_i(\vec{x}, t) = T_w^* (w_i + w_{\tilde{i}}) - g_i(\vec{x}, t) \tag{31}$$

And for adiabatic walls:

$$g_i(\vec{x}, t) = g_i(\vec{x} + \vec{c}_{i,n} \delta t, t) \tag{32}$$

Which n is the direction perpendicular to the wall.

3. Results

3.1. Grid study

A grid analysis has been done on this problem to find the optimal solution grid since the LBM is a numerical technique that has been used to describe the heat transfer of PCMs. It has been examined utilizing

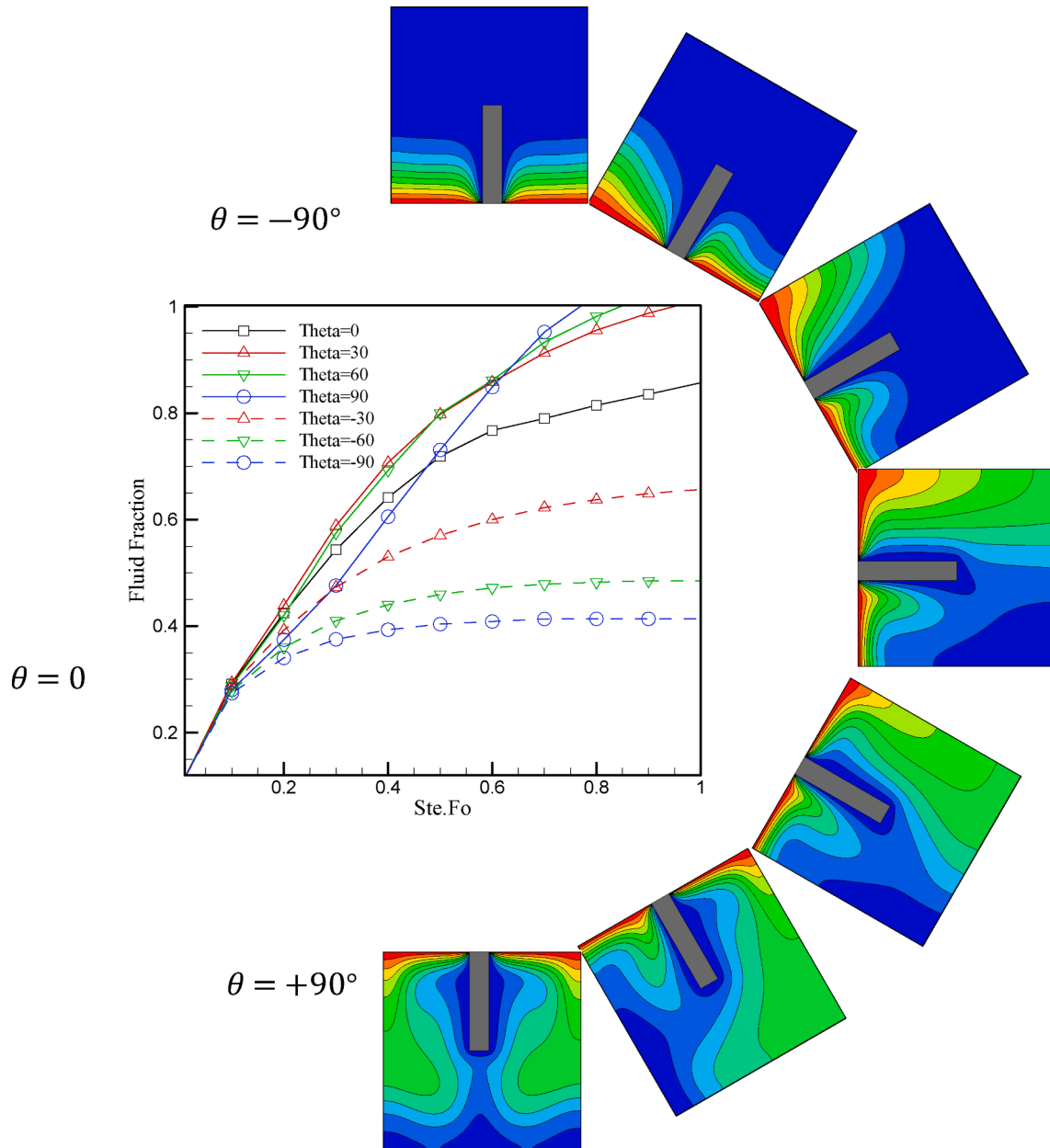


Fig. 14. Isotherms at $Ra = 10^5$ at different angles $\theta = -90^\circ$ to 90° in an adiabatic cavity with an adiabatic fin on the heated wall.

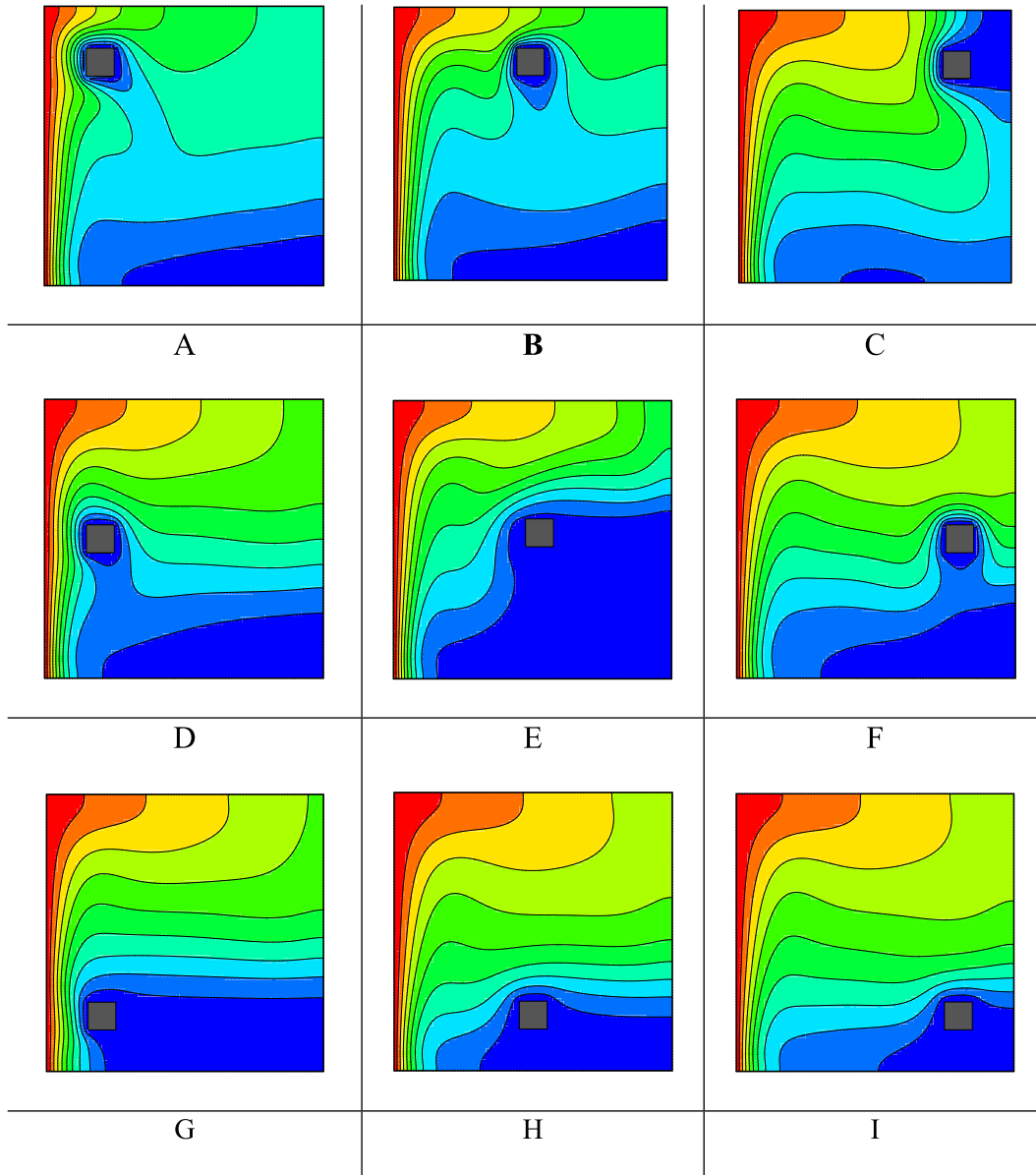


Fig. 15. Isotherms at $Ra = 10^5$ and zero enclosure angle in the presence of an adiabatic obstacle in different positions.

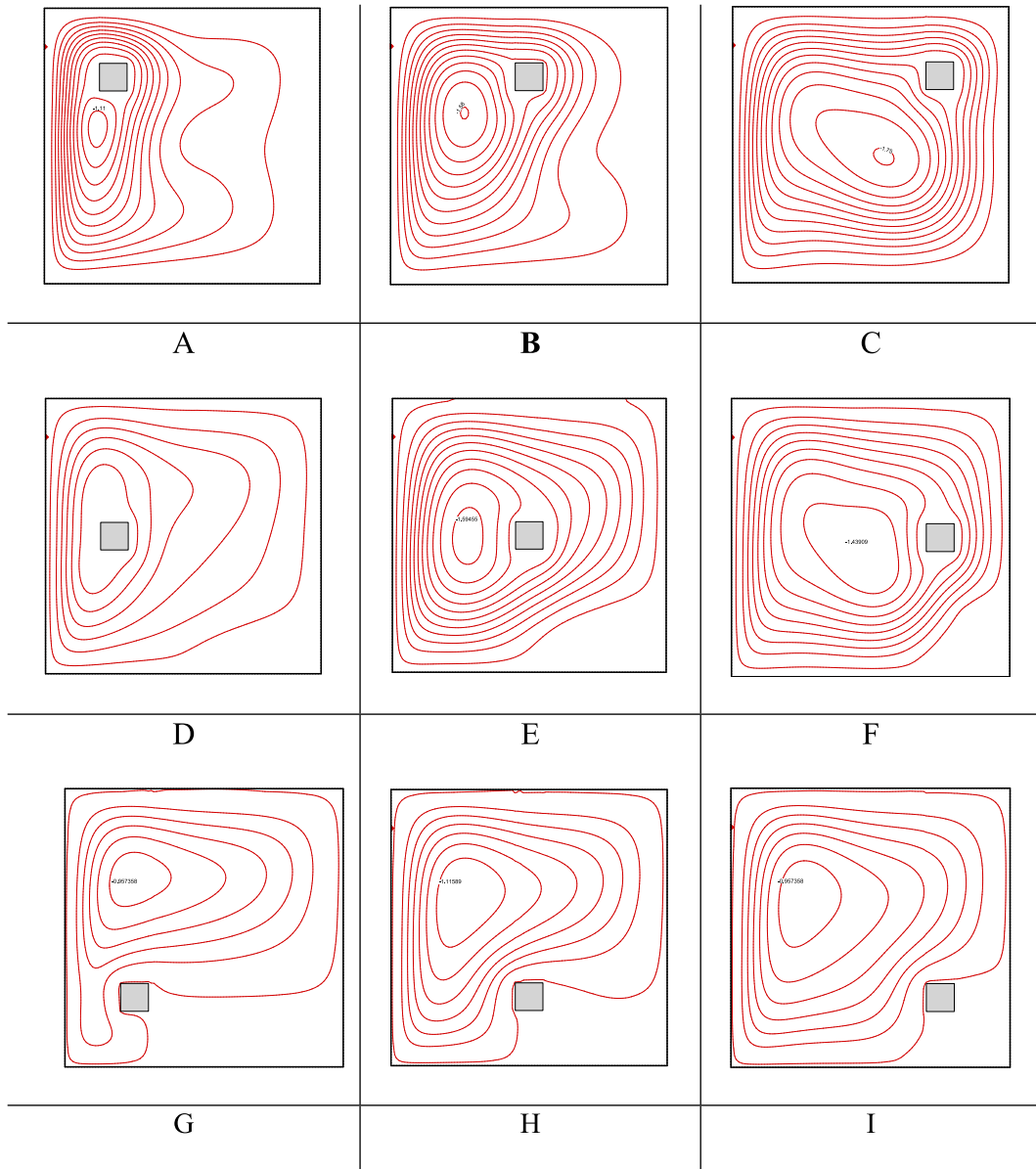


Fig. 16. Streamlines at $Ra = 10^5$ and zero enclosure angle in the presence of an adiabatic obstacle in different positions.

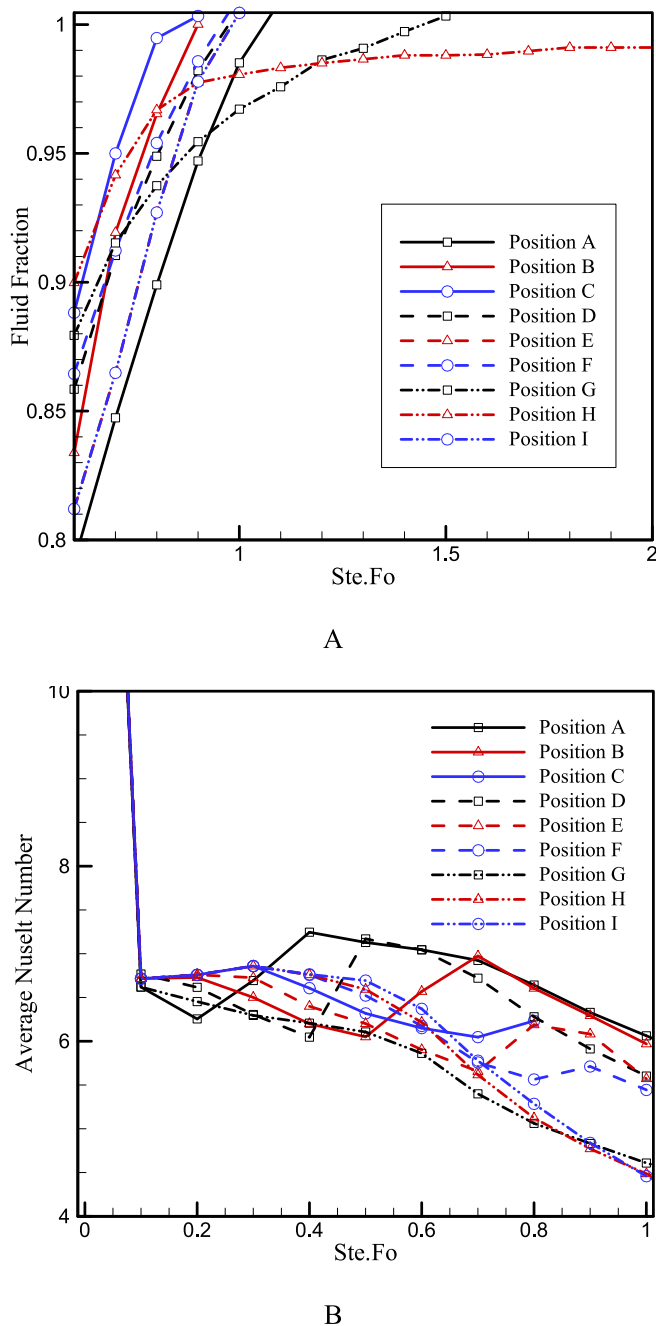


Fig. 17. (A) Fluid fraction diagram and (B) Average Nusselt number according to $Ste.Fo$ number in $Ra = 10^5$ and the cavity in line with the horizon in different obstacle positions.

PCM-containing 50×50 , 100×100 , 150×150 , 200×200 , and 250×250 grids. This was accomplished by plotting the average Nusselt number at various $Ste.Fo$ values and comparing the results in Fig. 3. In all cases in this paper T_c is considered to be equal to melting temperature (T_m). In the grid study, Fig. 3 reveals that the average Nusselt number diagram stabilizes and remains constant after a grid resolution of 200×200 . Hence, we have chosen this grid size for our simulations to strike a balance between accuracy and computational efficiency.

3.2. Validation

In the validation process of our developed numerical code using the Lattice Boltzmann Method's (LBM) thermal model, we compared our

findings with results from other reputable sources to assess the program's accuracy. Particularly, we compared the average Nusselt number obtained in our investigation with that of Jourabian et al. [31], who modeled natural heat transfer in a square cavity containing Phase Change Materials (PCMs) at $Ra = 10^5$ and $Ste = 10$. Fig. 4 displays the average Nusselt number of PCM versus $Ste.Fo$ number, allowing for a direct comparison of the results. The maximum discrepancy between the values was only 3%, indicating a significant agreement between our findings and the referenced study. Additionally, we compared streamlines and isothermal lines at $Ra = 1.7 \times 10^5$, as shown in Fig. 5, which further demonstrates excellent concurrence between our results and the reference data.

3.3. Effect of Ra number

In this section, the outcomes for the topic covered in this paper are contrasted using various Rayleigh numbers. In this section, the findings for three conditions—without adiabatic fin and obstacle, adiabatic obstacle presence, and adiabatic fin presence—were analyzed and contrasted. The isotherms and fluid fraction diagram in a square cavity filled with PCMs without utilizing fins are shown in this section for $Ra = 10^3$ – 10^5 . The findings in Figs. 6 and 7 indicate that the PCM becomes fluid more quickly when the Ra number is raised from $Ra = 10^3$ to $Ra = 10^5$. This implies that PCMs melts faster as the Ra number rises which comes from the fact that in higher Ra numbers natural convection is more powerful. By increasing the Ra number from $Ra = 10^3$ to $Ra = 10^5$ the melting time decreases from $Ste \times Fo = 0.3$ to $Ste \times Fo = 0.9$. The presented figure depicts dimensionless temperature contours at various dimensionless times. Initially, isothermal lines are vertical, indicating minimal natural convection influence. Over time, the impact of natural convection intensifies, particularly at higher Rayleigh numbers (Ra). This leads to enhanced heat transfer from the left wall, causing the generated heat to penetrate deeper into the Phase Change Material (PCM), resulting in faster melting. This observation emphasizes the significant role of natural convection and its augmentation with higher Ra numbers, influencing the efficiency of PCM melting processes.

Figs. 8 and 9 show the effect of the Ra number in a cavity with an adiabatic fin. As a result, only 60% of the PCM is converted to a liquid state when the Ra number is equal to 10^3 or 10^4 . However, when $Ra = 10^5$, the complete melting time increases from 0.9 to 2, which is a doubling of the melting time. Therefore, the presence of the fin completely increases the efficiency of the PCM. Additionally, by comparing the Isotherms with the results of the cavity without a fin, it is obvious that the adiabatic fin is completely effective in melting patterns.

Similarly, when an adiabatic obstacle is in the cavity, the obstacle affects the melting process and delays melting. In this case, at $Ra = 10^3$ and $Ra = 10^4$, the PCM does not melt completely as well (Figs. 10 and 11).

3.4. Effect of cavity angle

In this part, it is studied how the cavity angle affects the cavity in three scenarios: one without an obstacle and an adiabatic fin, one with an adiabatic obstacle, and one with an adiabatic fin. The Ra number is set to $Ra = 10^5$ in the simulations below, while the Stefan number is set to $Ste = 10$. Angles between -90 and 90° were used to investigate the findings. The lengths of the fin and obstacle are set to $L_f = 0.5$ and $L_o = 0.1$ respectively.

In the absence of adiabatic obstacles and fins, Fig. 12 shows a profound sensitivity of the isothermal lines to the orientation of the cavity. A transition from a cavity angle of 0 to -90° induces a notable delay in the melting process. This delay can be attributed to the counter-directional heat transfer relative to gravitational forces. The distribution of isothermal lines corroborates this phenomenon, as cavity angle adjustments flatten the gradient of isothermal lines. At $\theta = 90^\circ$, all isothermal lines uniformly flatten, resembling scenarios marked by

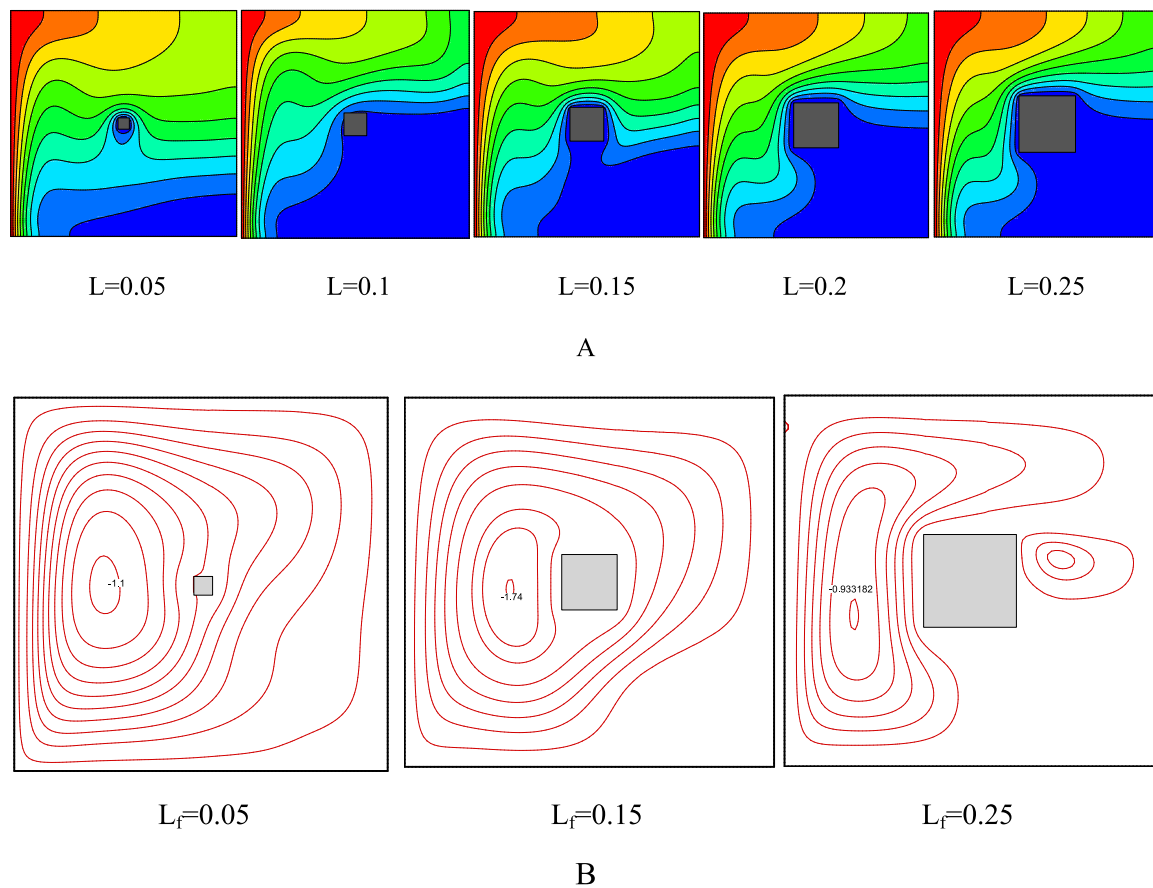


Fig. 18. (a) Isotherms and (b) streamlines at Rayleigh number $Ra = 10^5$ and zero cavity angle in the presence of adiabatic obstacle of different sizes $L = 0.05$ – 0.25 .

minimal convection within the cavity's heat transfer dynamics.

For cases of $\theta = 30^\circ$ and $\theta = 60^\circ$, the melting process accelerates, whereas cavity rotation in the opposite direction introduces a melting delay. Notably, at $\theta = 90^\circ$, a distinct and abrupt increase in the fluid fraction diagram's slope emerges beyond $Ste.Fo = 0.6$, underscoring evolving dynamics (See Figs. 13 and 14).

In the scenario involving an adiabatic obstacle, both the melting process and the configuration of isothermal lines remain consistent.

In the context of the adiabatic fin scenario, the process of melting is observed to accelerate in positive angles while being potentially delayed in negative angles. Particularly noteworthy is the situation at $\theta = 90^\circ$, representing the cavity's upper wall as the melting surface. Here, the presence of an adiabatic fin notably expedites the PCM melting process.

A comprehensive analysis of all outcomes reveals a consistent trend: the implementation of an adiabatic fin or obstacle can effectively delay the melting process by up to 50%.

3.5. Effect of obstacle's size and position

In this part, the adiabatic obstacle was put in various locations and with varying sizes in the solution domain to examine its impact on the melt rate and isotherms. This investigation aims to determine the impact of the size and location of the adiabatic obstacle on the cavity. In this study, the cavity's inclination is equal to 0° , and the Ra number is set at $Ra = 10^5$. Fig. 15 demonstrates how the PCM melts in various adiabatic obstacle positions.

As illustrated in Fig. 15, the placement of the adiabatic obstacle completely affects how the PCM melts, and the location of the adiabatic obstacle determines where the fluid's final melting point occurs. Incorporating an adiabatic obstacle generates an unmelted zone around the obstacle, resulting in this region being the last to undergo melting

within the cavity. This characteristic holds significance in specific applications, such as those involving electric chips or delicate devices requiring protection from heat generated by adjacent sources.

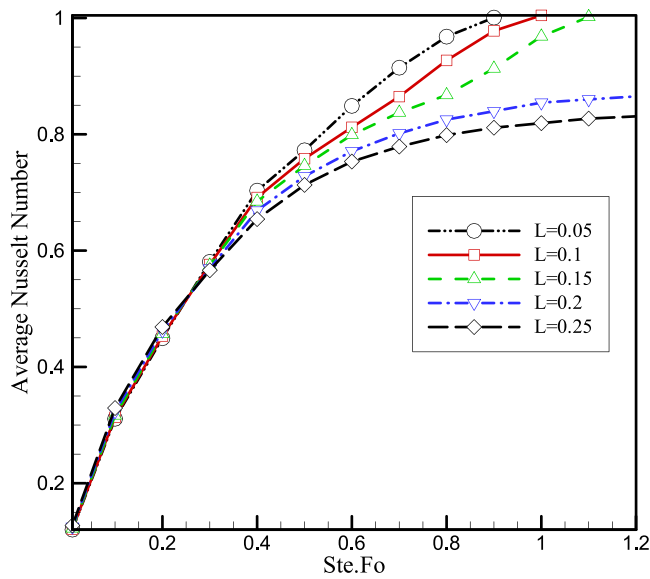
The streamlines in the cavity are shown in Fig. 16 in a variety of states, each corresponding to a unique configuration of the obstacle. This figure demonstrates that the presence of an adiabatic barrier between a cold wall and a hot wall always results in the formation of a vortex close to the hot wall, which prevents heat from penetrating the cold region upstream of the adiabatic obstacle. This is the case regardless of the specific circumstances.

Fig. 17 illustrates variations in fluid fraction and average Nusselt number across different $Ste.Fo$ numbers. The findings indicate that the PCM experiences earlier melting in upper obstacle positions, specifically in locations A, B, and C. Furthermore, the proximity of the adiabatic fin to the cold wall correlates with an accelerated melting process. This phenomenon is supported by higher average Nusselt numbers in upper positions, signifying enhanced heat transfer and consequently expediting the PCM melting.

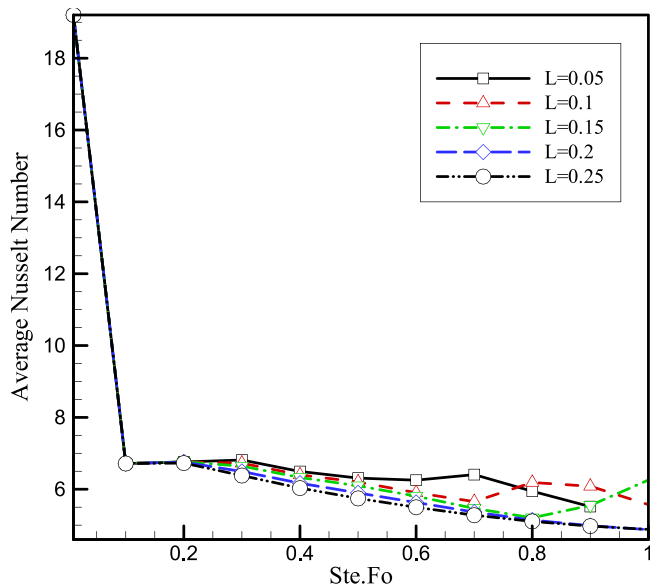
The impact of the adiabatic obstacle's size on the melting of the PCM is seen in Fig. 18. This graph demonstrates how the influence of the adiabatic obstacle on melting form rises as the adiabatic obstacle gets bigger. This diagram demonstrates how the melting cannot proceed if the adiabatic obstacle has a value of $L_f = 0.25$. Fig. 19 demonstrates that complete melting does not take place in the cavity when $L_f > 0.1$ and that as the size of the obstacle rises, the amount of melted material in the cavity increases.

Observing the flow lines around the obstacle reveals that as the cavity expands, a large vortex forms on the side of the hot wall, and this vortex becomes stronger as the cavity expands, preventing the heat flow from the hot wall from entering the hollow's rear.

The size of the adiabatic obstacle exhibits a clear impact on the



A



B

Fig. 19. Melting rate diagram according to $Ste.Fo$ number in $Ra = 10^5$ and the cavity in line with the horizon in different obstacle sizes.

melting process, with larger obstacles resulting in delayed melting. Interestingly, up to a point where around 60% of the PCM is melted, the melting time remains constant. However, beyond this threshold, the size of the adiabatic obstacle becomes a determinant factor. Notably, an increase in the size of the adiabatic obstacle correlates with a decrease in the average Nusselt number, underlining the diminishing efficiency of heat transfer as the obstacle size increases.

3.6. Effect of Fin's size and position

This section looks at how an adiabatic fin affects the isotherms and the rate at which PCMs melt. Fig. 20-a shows isotherms in different positions of the adiabatic fin. The findings are first given at various heights for the scenario where the fin length is equal to $L_f = 0.5$. The

Rayleigh number in this simulation was $Ra = 10^5$, and the angle of the cavity about the horizon was set at 0. The findings demonstrate that it is possible to alter the PCM melting pattern by raising the height of the adiabatic fin. As can be observed, while the fin is at $Y_f = 0.1$, melting begins at the top of the cavity and concludes at its bottom, however at $Y_f = 0.7$, the last area of the cavity where the solid transform into liquid is the higher part close to the cold wall. Fig. 20-b demonstrates fluid fraction of every case in different $Ste.Fo$ numbers. It shows that when $Y_f < 0.3$ the PCM in the cavity does not melt completely. It means when the adiabatic fin is in lower heights, the PCM can absorb more energy. When approximately 80% of the PCM is melted, a noteworthy observation emerges: altering the height of the fin from $Y_f = 0.1$ to $Y_f = 0.7$ leads to a doubling of the melting time. Furthermore, decreasing the fin height from 0.5 to 0.7 results in an extended complete melting time, with an increase of around 10 percent. These findings emphasize the substantial influence of fin height on the melting process, underlining the pivotal role of this parameter in shaping PCM behavior during phase change.

Fig. 20-c provides clear evidence that elevating the height of the adiabatic fin leads to a notable increase in the average Nusselt number along the hot wall. This phenomenon arises due to the emergence of larger vortex structures behind the fin at higher fin heights. As these vortices intensify, they enhance convective heat transfer, resulting in the observed elevation of the average Nusselt number on the hot wall.

Fig. 22 shows the fluid fraction diagram and isothermal contours for the case where the adiabatic fin is placed in the middle of the hot wall at different lengths. According to the figure shown, with the increase in fin length, the melting pattern is affected by fin length, but no change is observed in the location of the last point where melting takes place. By examining the diagram of the fluid component, it can be seen that the melting process is delayed by increasing the fin length so that at $L_f > 0.5$, all the heat is absorbed in the fluid.

Fig. 21 depicts the flow lines for three sizes of fins. This image demonstrates that as the length of the fin rises, two vortices are produced above and below it, which prevents the hot flow from moving to the front of the fin. As a result, the front of the fin melts at a very low pace, which may be described as “slowly” melting. After a certain amount of time, the melting process ceases.

4. Conclusion

This study uses an enthalpy-based LBM in a cavity to model the melting process of PCM. The simulations are done in three scenarios using adiabatic obstacles and fin. The impact of several factors, including the Ra number, cavity angle, and fin and obstacle's fin and obstacle, is considered. The findings of this research will contribute to enhancing mechanical PCM-based mechanical systems to delay melting time. The findings of this paper are as follows:

- Higher Ra numbers facilitated faster melting due to intensified natural convection, with the efficiency of PCM melting processes notably influenced by the introduction of adiabatic fins and obstacles. This comprehensive examination contributes to our understanding of PCM melting dynamics under varying conditions, highlighting the significance of natural convection and geometric modifications for thermal energy storage and related applications. The melting time falls from $Ste \times Fo = 3.0$ to $Ste \times Fo = 0.9$ by raising Ra from $Ra = 10^3$ to $Ra = 10^5$.
- The absence of adiabatic obstacles and fins led to a remarkable orientation-driven impact on isothermal lines and melting times. Positive angles accelerated melting, while negative angles caused potential delays. The adiabatic fin scenario expedited melting at positive angles and delayed it at negative angles. Overall, the study establishes a significant link between cavity orientation, adiabatic features, and PCM melting dynamics, providing insights for practical applications.

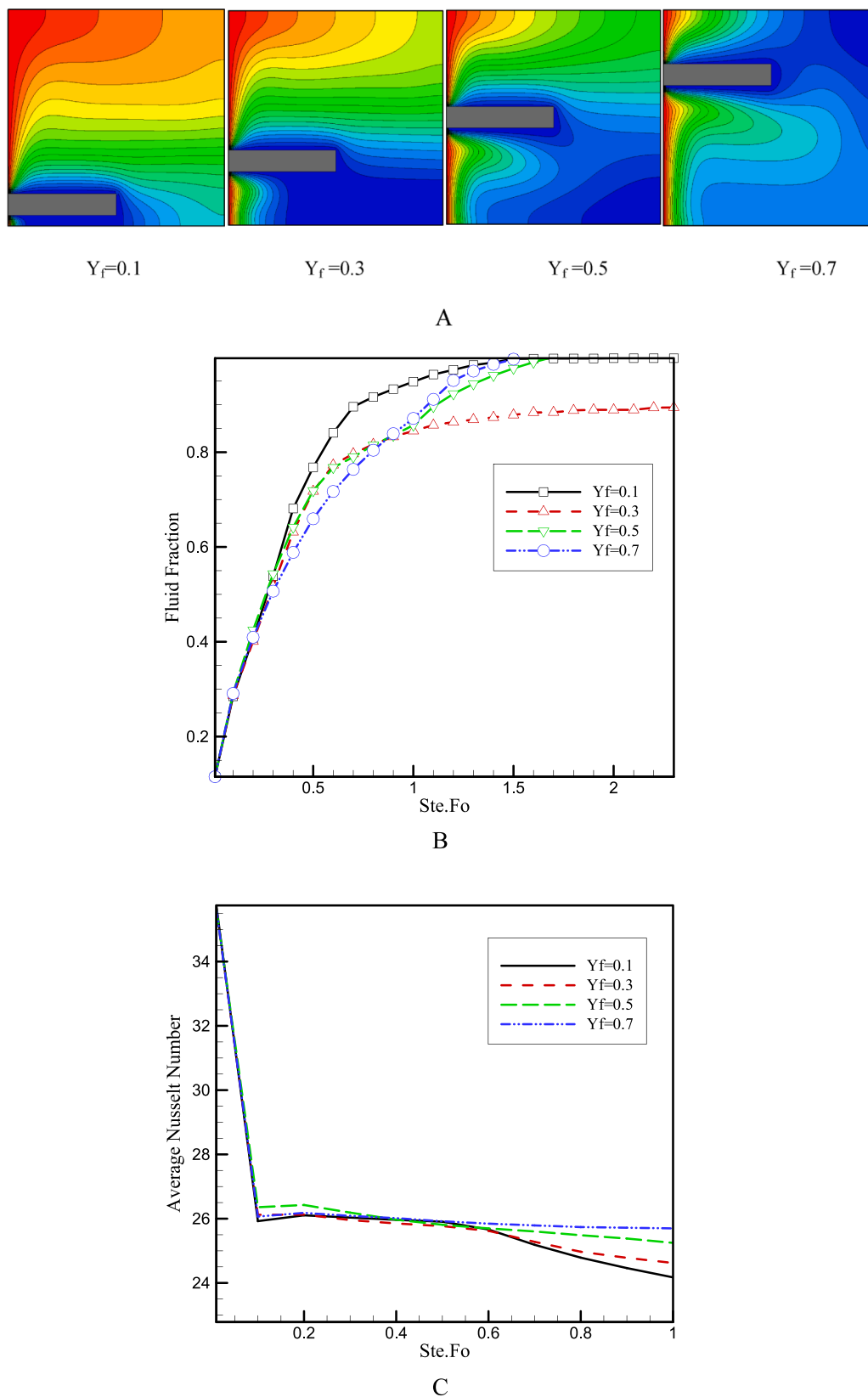


Fig. 20. (a) Isotherms and (b) Fluid Fraction diagram (c) Average Nusselt number at $Ra = 10^5$ and zero cavity angle in the presence of adiabatic obstacle of different heights $L_f = 0.05-0.25$.

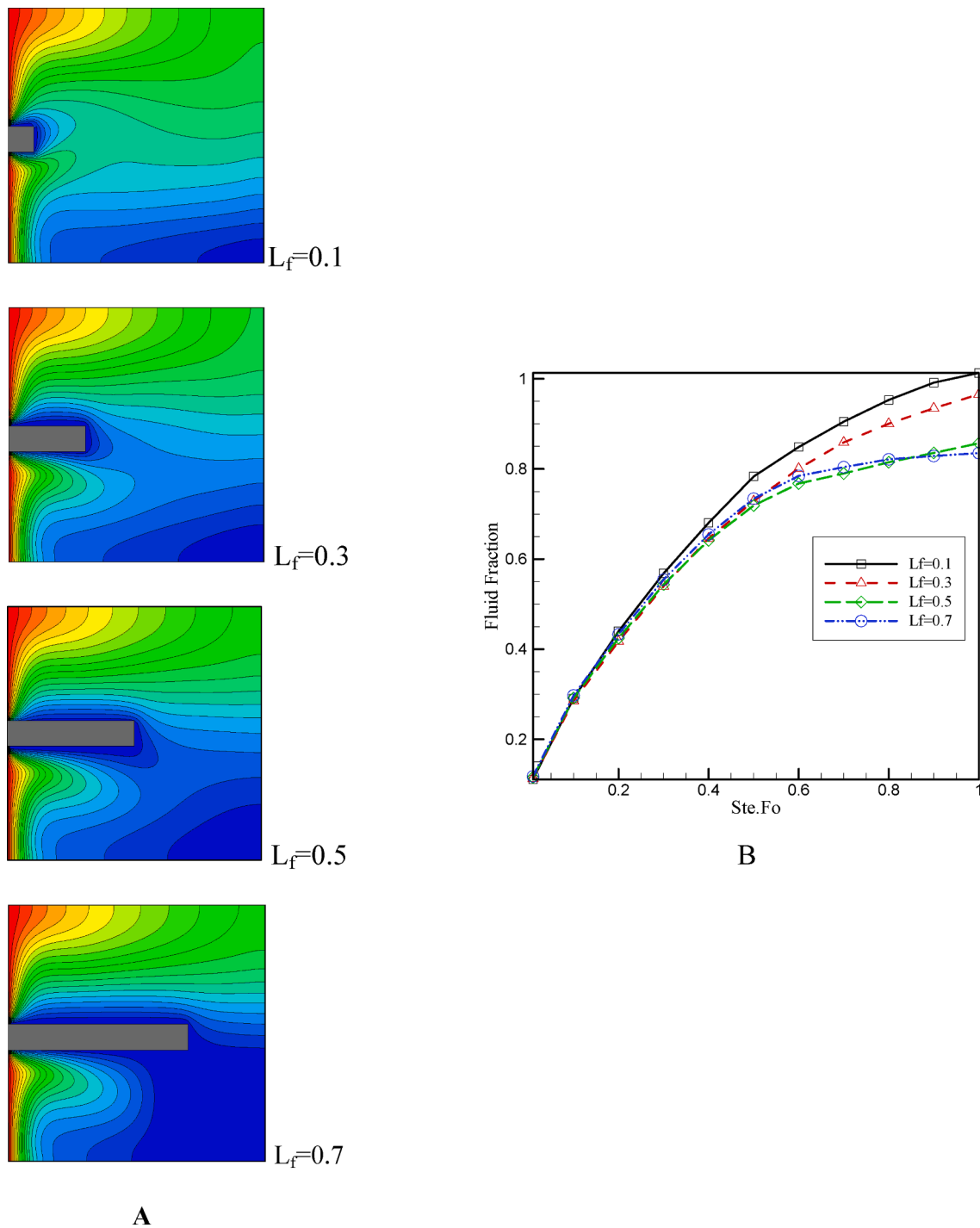


Fig. 21. (a) Isotherms and (b) Fluid Fraction diagram at $Ra = 10^5$ and zero cavity angle in the presence of adiabatic fin of different Lengths $L_f = 0.1-0.7$.

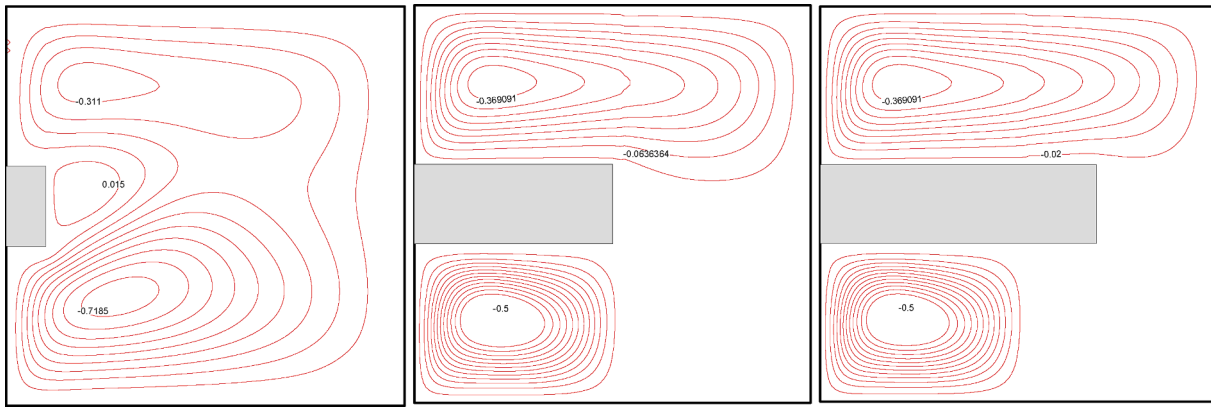


Fig. 22. Streamlines at $Ra = 10^5$ and zero cavity angle in the presence of adiabatic fin of different Lengths $L_f = 0.1, 0.5$ and 0.7 .

- The adiabatic obstacle's positioning profoundly influences PCM melting dynamics, determining the location of the final melting point and creating protected zones with delayed melting. Streamline patterns consistently reveal the formation of a heat-impeding vortex near the hot wall due to the adiabatic barrier.
- The role of upper obstacle positions and adiabatic fin proximity in accelerating PCM melting, supported by enhanced heat transfer and average Nusselt numbers. These findings collectively contribute to a comprehensive understanding of how geometric features impact PCM behavior, informing practical applications in thermal management and protection.
- Full melting is not achieved in the presence of an adiabatic obstacle exceeding $L_f > 0.1$, with larger obstacles increasing the volume of melted material. The flow pattern analysis reveals the emergence of a robust vortex near the hot wall as the cavity expands, hindering heat transfer from the hot wall's rear. Larger adiabatic obstacles lead to delayed melting, notably beyond the 60% PCM melting point, and a subsequent decline in average Nusselt number underscores the reduced heat transfer efficiency associated with larger obstacles.
- The figure demonstrates that while the melting pattern is influenced by fin length, the location of the last melting point remains unchanged. Examination of the fluid component diagram reveals a delayed melting process associated with increased fin length, where complete heat absorption occurs at $L_f > 0.5$.

Declaration of Competing Interest

The authors declare that they have no known competing financial interests or personal relationships that could have appeared to influence the work reported in this paper.

Acknowledgement

This work was supported by Sichuan Province Luzhou city of Stars science and technology planning project(2022-GYF-16) and (2022-JYJ-129), Scientific research and innovation team construction project of Luzhou vocational and Technical College (2021YJTD07).

References

- [1] K. Natesan, S. Karinka, A comprehensive review of heat transfer enhancement of heat exchanger, heat pipe and electronic components using graphene, *Case Stud. Therm. Eng.* 45 (2023), <https://doi.org/10.1016/j.csite.2023.102874>.
- [2] R. Samanta, H. Chattopadhyay, C. Guha, A review on the application of lattice Boltzmann method for melting and solidification problems, *Comput. Mater. Sci* 206 (2022), <https://doi.org/10.1016/j.commatsci.2022.111288>.
- [3] F. Li, et al., Application and analysis of flip mechanism in the melting process of a triplex-tube latent heat energy storage unit, *Energy Rep.* 9 (2023) 3989–4004, <https://doi.org/10.1016/j.egy.2023.03.037>.
- [4] M.A. Alazwari, M. Algarni, M.R. Safaei, Effects of various types of nanomaterials on PCM melting process in a thermal energy storage system for solar cooling application using CFD and MCMC methods, *Int. J. Heat Mass Transf.* 195 (Oct. 2022), <https://doi.org/10.1016/j.ijheatmasstransfer.2022.123204>.
- [5] A. Mourad, et al., Numerical study on n-octadecane PCM melting process inside a pear-shaped finned container, *Case Studies in Thermal Engineering* 38 (Oct. 2022), <https://doi.org/10.1016/j.csite.2022.102328>.
- [6] M. Jourabian, A.A.R. Darzi, D. Toghraie, O Ali Akbari, Melting process in porous media around two hot cylinders: Numerical study using the lattice Boltzmann method, *Physica A* 509 (2018) 316–335.
- [7] S. John, K. Sreyas, Y. Mohan, A.D. Thampi, S. Rani, Numerical investigation on the effect of PCM thickness and nano-additive on the cooling performance of Stearic Acid based battery thermal management system, *Mater. Today: Proc.* (Jan. 2023), <https://doi.org/10.1016/j.matpr.2023.01.267>.
- [8] M. Nemati, A.R.S.N. Abady, D. Toghraie, Numerical investigation of the pseudopotential lattice Boltzmann modeling of liquid–vapor for multi-phase flows, *Physica A* 489 (2018) 65–77.
- [9] A. Alagumalai et al., “Nano-engineered pathways for advanced thermal energy storage systems,” *Cell Reports Physical Science*, vol. 3, no. 8. Cell Press, Aug. 17, 2022. doi: 10.1016/j.xcrp.2022.101007.
- [10] A.A. Balootaki, A. Karimipour, D. Toghraie, Nano scale lattice Boltzmann method to simulate the mixed convection heat transfer of air in a lid-driven cavity with an endothermic obstacle inside, *Physica A* 508 (2018) 681–701.
- [11] A. Toghianiyan, M. Zarringhalam, O.A. Akbari, G.A.S. Shabani, D. Toghraie, Application of lattice Boltzmann method and spinodal decomposition phenomenon for simulating two-phase thermal flows, *Physica A* 509 (2018) 673–689.
- [12] M.H. Shojaeefard, M. Jourabian, A.A. Rabienataj Darzi, Rectangular heat sink filled with PCM/ hybrid nanoparticles composites and cooled by intruded T-shaped cavity: Numerical investigation of thermal performance, *Int. Commun. Heat Mass Transfer* 127 (Oct. 2021), <https://doi.org/10.1016/j.icheatmasstransfer.2021.105527>.
- [13] M.H. Shojaeefard, M. Jourabian, A.A. Rabienataj Darzi, Interactions between hybrid nanosized particles and convection melting inside an enclosure with partially active walls: 2D lattice Boltzmann-based numerical investigation, *Heat Transfer* 50 (5) (Jul. 2021) 4908–4936, <https://doi.org/10.1002/htj.22109>.
- [14] H. Liu, J. Jiang, S. Zhan, X. Yang, D. Yu, G. Yan, Study on energy management model of integrated New Energy-Storage-Charging system considering the influence of uncertainties, *Fuel* 331 (Jan. 2023), <https://doi.org/10.1016/j.fuel.2022.125784>.
- [15] A. Laouer, M. Teggat, E. Tunçbilek, M. Arıcı, L. Hachani, K.A.R. Ismail, Melting of hybrid nano-enhanced phase change material in an inclined finned rectangular cavity for cold energy storage, *J Energy Storage* 50 (Jun. 2022), <https://doi.org/10.1016/j.est.2022.104185>.
- [16] F. Souayfane, P.H. Biwole, F. Fardoun, Melting of a phase change material in presence of natural convection and radiation: A simplified model, *Appl. Therm. Eng.* 130 (2018) 660–671, <https://doi.org/10.1016/j.applthermaleng.2017.11.026>.
- [17] B. Peng, M. Qiu, N. Xu, Y. Zhou, W. Sheng, F. Su, Optimum orthogonally structured fins in charging enhancement of phase change materials (PCMs): PCMs' thermophysical properties effects, *Int. J. Therm. Sci.* 184 (2023), <https://doi.org/10.1016/j.ijthermalsci.2022.108005>.
- [18] K. Luo, A.T. Pérez, J. Wu, H.L. Yi, H.P. Tan, Efficient lattice Boltzmann method for electrohydrodynamic solid-liquid phase change, *Phys. Rev. E* 100 (1) (2019), <https://doi.org/10.1103/PhysRevE.100.013306>.
- [19] Z. Rui, J. Li, J. Ma, H. Cai, B. Nie, H. Peng, Comparative study on natural convection melting in square cavity using lattice Boltzmann method, *Results Phys.* 18 (Sep. 2020), <https://doi.org/10.1016/j.rinp.2020.103274>.
- [20] X. Zhang, et al., Numerical study of mixed convection of nanofluid inside an inlet/outlet inclined cavity under the effect of Brownian motion using Lattice Boltzmann Method (LBM), *Int. Commun. Heat Mass Transfer* 126 (2021), <https://doi.org/10.1016/j.icheatmasstransfer.2021.105428>.
- [21] M. Sheikholeslami, S.A. Shehzad, F.M. Abbasi, Z. Li, Nanofluid flow and forced convection heat transfer due to Lorentz forces in a porous lid driven cubic enclosure with hot obstacle, *Comput. Methods Appl. Mech. Eng.* 338 (2018) 491–505, <https://doi.org/10.1016/j.cma.2018.04.020>.

- [22] Y. Zhao, B. Shi, Z. Chai, L. Wang, Lattice Boltzmann simulation of melting in a cubical cavity with a local heat-flux source, *Int. J. Heat Mass Transf.* 127 (2018) 497–506, <https://doi.org/10.1016/j.ijheatmasstransfer.2018.06.116>.
- [23] M. Sheikholeslami, M. Seyednezhad, Lattice Boltzmann method simulation for CuO-water nanofluid flow in a porous enclosure with hot obstacle, *J. Mol. Liq.* 243 (2017) 249–256, <https://doi.org/10.1016/j.molliq.2017.08.038>.
- [24] A. Rebey, S.M. Sajadi, Examine the lattice Boltzmann method for the mixed convection simulation of water/Al₂O₃ nanofluid in a 2D rectangular cavity under radiation with isothermal semicircular obstacles, *Eng. Anal. Bound. Elem.* 149 (2023) 27–37, <https://doi.org/10.1016/j.enganabound.2023.01.009>.
- [25] Q. Ren, C.L. Chan, GPU accelerated numerical study of PCM melting process in an enclosure with internal fins using lattice Boltzmann method, *Int. J. Heat Mass Transf.* 100 (2016) 522–535, <https://doi.org/10.1016/j.ijheatmasstransfer.2016.04.059>.
- [26] F. Talati, M. Taghilou, Lattice Boltzmann application on the PCM solidification within a rectangular finned container, *Applied Thermal Engineering* 83 (2015) 108–120, <https://doi.org/10.1016/j.applthermaleng.2015.03.017>.
- [27] Z. Rui, J. Li, T. Ding, J. Ma, H. Peng, Research on thermal performance and optimization design of phase change pin fin heat sink based on Lattice Boltzmann method, *J Energy Storage* 55 (2022), <https://doi.org/10.1016/j.est.2022.105659>.
- [28] F. Zhang, A. Lin, P. Wang, P. Liu, Optimization design of a parallel air-cooled battery thermal management system with spoilers, *Appl. Therm. Eng.* 182 (2021), <https://doi.org/10.1016/j.applthermaleng.2020.116062>.
- [29] G. Feng, Y. Feng, L. Qiu, X. Zhang, Evaluation of thermal performance for bionic porous ceramic phase change material using micro-computed tomography and lattice Boltzmann method, *Int. J. Therm. Sci.* 179 (2022), <https://doi.org/10.1016/j.ijthermalsci.2022.107621>.
- [30] W.S. Jiaung, J.R. Ho, C.P. Kuo, Lattice Boltzmann method for the heat conduction problem with phase change, *Numerical Heat Transfer, Part B: Fundamentals* 39 (2) (2001) 167–187, <https://doi.org/10.1080/10407790150503495>.
- [31] M. Jourabian, M. Farhadi, A.A.R. Darzi, Simulation of natural convection melting in an inclined cavity using lattice Boltzmann method, *Scientia Iranica* 19 (4) (2012) 1066–1073, <https://doi.org/10.1016/j.scient.2012.06.014>.